arXiv:1411.0008v1 [cond-mat.mes-hall] 31 Oct 2014

Theory of Transport Phenomena in Coherent Quantum Hall Bilayers

I. Sodemann,[1] Hua Chen,[2] and A. H. MacDonald[2]

[1] *Department of Physics, Massachusetts Institute of Technology, Cambridge, Massachusetts 02139*
[2] *Department of Physics, University of Texas at Austin, Austin, Texas 78712*

(Dated: February 19, 2022)

We argue that all anomalous transport properties of coherent quantum quantum Hall bilayers can be understood in terms of a mean-field transport theory in which the condensate phase is nearly uniform across the sample, and the strength of condensate coupling to interlayer tunneling processes is substantially reduced compared to the predictions of disorder-free microscopic mean-field theory. These ingredients provide a natural explanation for recently established I-V characteristics which feature a critical current above which the tunneling resistance abruptly increases and a non-local interaction between interlayer tunneling at the inner and outer edges of Corbino rings. We propose a microscopic picture in which disorder is the main agent responsible for the reduction of the effective interlayer tunneling strength.

PACS numbers: 73.43.-f, 73.43.Lp, 03.75.Lm, 73.43.Jn

I. INTRODUCTION

The discovery a number of years ago by Spielman *et al.* [1] of a huge enhancement of the zero-bias tunneling conductance between two nearby two-dimensional-electron layers provided compelling evidence for an interesting ordered state in which interlayer phase coherence is established spontaneously [2, 3]. This tunneling anomaly has so far been observed only in the quantum Hall regime and only near total Landau level filling factor $\nu_T = 1$. The ordered state can be viewed as a condensate formed from electrons in the lowest Landau level of one layer and holes in the lowest Landau level of the other layer. Other striking transport anomalies are characteristic the same ordered state, including quantized Hall drag [4], vanishing Hall and longitudinal resistances [5–7] when Hall bar bilayers are contacted so that opposite layers carry currents in opposite directions, and excitonic Andreev scattering [8] and nearly perfect Coulomb drag in Corbino geometry bilayers [9].

A bilayer state with spontaneous interlayer phase coherence is equivalent to a state with a condensate of spatially indirect excitons. Prior to Spielman *et al.*'s work the appearance of this unusual type of broken symmetry in quantum Hall bilayers had been predicted [10] on the basis of microscopic considerations particular to the quantum Hall regime, hinted at experimentally [11, 12], and studied theoretically [13–22]. The most spectacular properties of these states were however not revealed until transport measurements were undertaken in which the two layers were independently contacted. The first of these [1] revealed the tunneling anomaly and stimulated a considerable body of additional theoretical work [23–44].

The relatively small value of the zero-bias tunneling conductance peak observed in early experiments, and its relatively weak dependence on in-plane magnetic field [45, 46], motivated theoretical researchers [23–25, 30–32, 36, 37, 39, 41, 43] to develop descriptions that started from the assumption that the interlayer coherent state lacked long-range order due to a combination of quantum and thermal order parameter fluctuations, and disorder. However, more recent experiments [8, 9, 46–52], often using four terminal measurement configurations to separate contact and tunneling resistances, have made it increasingly clear that the zero-bias tunnel conductance is at least as large as $\sim 250e^2/h$ and possibility much larger. These experiments also provided strong evidence for the presence of a critical inter-layer current which becomes sharp in the low temperature limit and is reminiscent of the critical current of a Josephson junction. When the critical current is exceeded the tunneling resistance abruptly increases. Most tellingly, experiments in

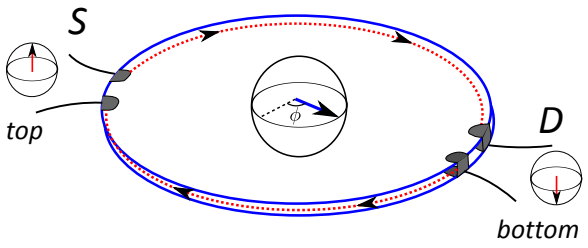


FIG. 1. Schematic illustration of the anomalous tunneling phenomena in coherent quantum Hall bilayers. A high chemical potential source is connected to the top layer and a low chemical potential drain is connected to the bottom layer. The layer pseudospin of transport electrons rapidly rotates from the layer-polarized source and drain orientations to the layer-coherent condensate orientations over small regions close to the contacts depicted by gray shading. Quasiparticle states in the source and drain electrodes are layer-localized and have pseudo spins which lie close to the north pole (for top layer electrodes) or to the south pole (for bottom layer states). The edge and bulk quasiparticle states in the condensate have coherent layer-delocalized wave functions and layer pseudo spins which lie close to the XY plane with a phase. Current experiments are consistent with an interlayer phase ϕ that is nearly uniform throughout the sample. Well formed quantum Hall plateaus demonstrate that transport electrons flow along sample edges. Corbino geometry samples have independent transport at inner and outer edges.

Corbino geometry samples [50, 51] have revealed a non-local interaction between tunneling characteristics at the sample's inner and outer edges. In particular, these experiments demonstrated that the critical current is determined by the sum [35] of the separate interlayer currents at the two independent edges. As we will explain, these results shed new light on the nature of the bilayer coherent state and directly demonstrate long-range coherence of the inter-layer phase.

We argue below that all transport anomalies which accompany quantum Hall bilayer exciton condensation (see Fig. 1), including the tunneling anomaly, can be described by combining a mean-field theory of electron-electron interactions with independent quasiparticle transport theory [16, 35, 42] and accounting for the influence of excitonic Andreev scattering on the interlayer phase [35]. We also propose new experiments which explore the time dependence of the condensate current-driven-dynamics and can be used both to further test our picture of bilayer exciton condensate transport anomalies and to quantify the order parameter energy functional it employs.

Our paper is organized as follows. In Section II we review the central ideas needed to understand the transport anomalies of bilayer exciton condensates. In Section III we describe transport in the macrospin limit in which the interlayer phase is constant across the sample, demonstrating that theoretical predictions in this limit achieve agreement with experiment for a variety of different measurement configurations. The spatial properties of the condensate depend on whether the length scale λ, defined by comparing the pseudospin stiffness parameter in the energy functional ρ with the tunneling parameter Δ which characterizes energetic preference for a particular interlayer phase value, is larger or smaller than the system size. The macrospin limit applies when λ is larger than the system size. In Section IV we consider the case in which λ is smaller than the system size. We demonstrate that the predictions of theory for this limit are in qualitative disagreement with recent experiments which have found the condensate state to be controlled by the sum of the currents at the inner and outer edges of Corbino-geometry samples. In Section V we explore the time dependence of the condensate dynamics, a regime of phenomena where experiments are still lacking. Comparison of theory and experiment for dynamical properties could be used to further deepen our understanding of bilayer exciton condensates, and in particular to test the theoretical framework we propose here. When microscopic mean-field theory is applied to disorder-free samples, the values predicted for Δ and ρ would not place experimental samples in the macrospin limit. In Section VI we discuss a picture for the microscopic origin of the dramatic reduction in Δ required to resolve this discrepancy. Its most important conclusion is that the phase appearing in Sections II-V should be understood as a coarse grained phase averaged over distances that are long compared to the disorder correlation length. Finally, we present our conclusions and summarize our findings in Section VII.

II. TRANSPORT THEORY

The phenomena we address have close analogies with spin-transfer torques and related effects in magnets and with tunneling in superconducting Josephson junctions. An order parameter for the pseudospin *which layer* degree-of-freedom can be defined as follows:

$$\mathbf{M} \equiv \frac{1}{2A} \sum_{k,\alpha\beta} \boldsymbol{\sigma}_{\alpha\beta} \langle c^\dagger_{k\alpha} c_{k\beta} \rangle, \tag{1}$$

where $c^\dagger, c$ are electron creation and annihilation operators, k is an intra-Landau-level orbital index, α, β run over top (t) and bottom (b) layer labels, and A is the area of the system. Following a standard procedure, an action describing the low energy dynamics can be constructed in terms of a local order parameter $\mathbf{M}(\vec{r}, t)$ whose magnitude remains constant while its orientation changes in space and time [21]. The corresponding Lagrangian density is:

$$\mathcal{L} = \hbar \dot{\phi}(\vec{r}, t) M_z(\vec{r}, t) - \mathcal{E}[\phi(\vec{r}, t), M_z(\vec{r}, t)], \tag{2}$$

where ϕ is the azymuthal angle of the local order parameter and M_z its projection along the z-axis, which is half of the electron density difference between the layers. In the zero temperature mean-field theory of the disorder-free $\nu_T = 1$ bilayer, all electrons share a common pseudospin state yielding a ground state with the maximum pseudospin polarization possible in the lowest Landau level Hilbert space: $|\mathbf{M}| = n/2$, where n is the electron density. More generally, one expects the order parameter to be reduced compared to this value as we discuss at length in Section VI.

The capacitive energy is assumed large enough to keep the order parameter in-plane: $M_z \ll |\mathbf{M}|$. The energy per unit area can then be written as:

$$\mathcal{E}[\phi, M_z] = -\Delta \cos\phi + \rho |\nabla \phi|^2 + \frac{e^2}{2c} M_z^2. \tag{3}$$

The first term arises from the single particle tunneling of electrons and it is controlled by the splitting, Δ_{SAS}, between (S) and antisymmetric (AS) double well states: $\Delta = \Delta_{\rm SAS} |\mathbf{M}|$. The second term captures the energy cost of spatial variation in interlayer phase characterized by ρ, the stiffness constant. The third term is the capacitive energy which is responsible for keeping the order parameter in the XY plane. Here c is the capacitance per unit area.

The non-dissipative dynamics of the phase follows from the Euler-Lagrange equations associated with $\mathcal{L}$. Dissipation arises when incoherent tunneling processes are accounted for [26] and the connection to external reservoirs

via electrical leads is included. The dynamics including these terms is described by:

$$\hbar \dot{M}_z = -\Delta \sin\phi + 2\rho\nabla^2\phi - \frac{g_{qp}}{A}\,\hbar\dot{\phi} + \sum_k \frac{\hbar I_k}{2} l_k \delta(\vec{r} - \vec{R}_k). \tag{4}$$

The first two terms in the right of the equation are non-dissipative and account respectively for coherent collective tunneling between layers and the divergence of the exciton supercurrent. The third term is a dissipative and accounts for incoherent tunneling between layers with a time-dependent interlayer phase. For simplicity we assume here that it is Ohmic allowing it to be characterized by an associated conductance g_{qp} measured in units of $e^2/\hbar$. This term can be understood by noting that $\hbar\dot{\phi}$ is equivalent to a chemical potential difference between the layers [53]. It is the layer pseudospin analog of Gilbert damping in a ferromagnet [54], and of the shunt resistance in the RCSJ model of a Josephson junction [55]. We have omitted an additional dissipative term proportional to $\nabla^2\dot{\phi}$ that would arise when the bulk of the quantum Hall liquid is not perfectly insulating [25].

The last term in Eq. (4) accounts for injection and removal of quasiparticles through layer-polarized contacts. As in the familiar case of superconducting Andreev scattering at NS interfaces, quasiparticle scattering off the order parameter violates particle number conservation (independent particle number in each layer in the present case) and is accompanied by a reaction effect which creates or annihilates excitons [35]. We assume the contacts are connected to the edge of the sample at positions R_k. In Eq. (4), I_k is the electron number current injected into the sample at contact k, and l_k takes values ± 1 for top and bottom layer contacts respectively. Assuming that quasiparticle interlayer coherence is established close to source and drain electrodes and integrating Eq. (4) over an small region Ω_k surrounding the contact [35, 40], we see that single-layer contacts effectively provide a Neumann type boundary condition for the normal derivative of the phase:

$$l_k \frac{\hbar I_k}{2} = -\oint_{\partial\Omega_k} ds\ \hat{n}\cdot(2\rho\nabla\phi). \tag{5}$$

Eq. (5) expresses the idea that the layer polarized quasiparticle current is converted into an excitonic supercurrent over a short microscopic distance. The conversion process which entails the creation or annihilation of interlayer excitons close to current sources and drains is analogous to Andreev scattering in superconductors and to spin-transfer torques in ferromagnets [35, 40].

So far we have discussed the equations which capture how transport currents influence the bilayer order parameter. The converse effect in which bilayer order influences transport, which is further detailed in the following sections, is even stronger and proceeds in the first place by establishing coherence between layers. In the quantum Hall regime the charge current flows from source to drain along chiral edge channels [56]. The source-to-drain conductance depends on contact details but is ideally $\sim e^2/h$ [42]. In a bilayer exciton condensate the edge states, like bulk states, are interlayer-coherent and have nearly equal magnitude amplitudes in the two layers. When the interlayer phase is time independent, voltage probes always measure the same voltage whether contacted to one layer or the other. When the interlayer phase is time-dependent but spatially constant, $\hbar\dot{\phi}/e$, contributes to interlayer voltages. This last effect is closely analogous [57] to spin-pumping [58, 59] in ferromagnets as we explain further below. Figure 1 summarizes transport in the coherent state.

III. MACROSPIN LIMIT

When the system is able to reach a time-independent steady state, the phase throughout the sample will satisfy a sine-Gordon equation:

$$\lambda^2\nabla^2\phi - \sin\phi = 0 \tag{6}$$

which must be solved together with the Neumann boundary conditions in Eq. (5). The length scale $\lambda = \sqrt{2\rho/\Delta}$ sets the typical scale over which the phase changes. In the limit in which the typical dimension of the sample is much smaller than λ, the phase of the condensate remains uniform throughout the sample. We refer to this as the *macrospin limit* in analogy with magnetism. In the macrospin limit the criterion for the existence of time-independent solutions to Eq. (4) reduces to:

$$\left| \sum_k l_k \frac{\hbar I_k}{2} \right| \leq A\Delta, \tag{7}$$

where A is the area of the sample. $\sum_k l_k \hbar I_k/2$ can be interpreted as the net rate at which layer pseudospin is transferred to the condensate by quasiparticle transport currents. Eq. 7 predicts that the critical current is proportional to sample area, as established experimentally in Ref. 60, and that it is the *total* layer polarized current injected or extracted out of the sample over all current contacts which controls the stability of time-independent solutions. This conclusion applies even if the sample is multiply connected, as it is the case in the Corbino geometry, and the currents are being injected simultaneously through otherwise disconnected edges. It is this recent experimental finding in Corbino samples [50, 51] which convincingly indicates that current experimental systems are effectively in the macrospin limit.

In the remainder of this section we assume the macrospin limit and demonstrate that the theory we have outlined is able to reproduce the shape of two- and four-terminal I-V characteristics. Assuming the system to

have a sufficiently strong capacitive energy to suppress the $\dot{M}_z$ term in Eq. (4), one obtains the following equation for the macrospin dynamics:

$$\frac{A\Delta}{\hbar}\sin\phi + g_{qp}\,\dot{\phi} - \sum_k l_k I_k/2 = 0. \tag{8}$$

In the two-terminal tunneling configuration where an electron number current I is driven from a source terminal connected to the top layer to a drain terminal along the same edge that is connected to the bottom layer, we have: $\sum_k l_k I_k/2 = I$. Denoting the chemical potential difference between source and drain by μ, one has:

$$\hbar I = g(\mu - \hbar\dot{\phi}), \tag{9}$$

where g is the two-terminal conductance in $e^2/\hbar$ units. The shift of the source-to-drain bias by $-\hbar\dot{\phi}$ captures the influence of the order parameter dynamics on the charge quasiparticle current flowing through the system edges. The $-\hbar\dot{\phi}$ shift in the interlayer bias can be understood by performing a unitary transformation to a rotating frame that transforms the quasiparticle Hamiltonian into a time-independent one [42]. This effect is the analog of the spin-pumping in metal spintronics [58, 59], and gives rise to an effective enhancement of the damping factor for the condensate phase: $g_{qp} \to g_{qp} + g$ [16].

The phase of the order parameter is time independent for $I < I_c$, with $\hbar I_c = A\Delta$. Over this range of current, the current-voltage characteristic is $\hbar I = g\mu$. When the bias exceeds a critical value $\mu > \mu_c \equiv \hbar I_c/g$, the phase starts to precess. By integrating Eq. (8) with respect to time we find that the average precession rate is:

$$\hbar\langle\dot{\phi}\rangle = \frac{g}{g_{qp}+g}\sqrt{\mu^2 - \mu_c^2}, \tag{10}$$

and that the two-terminal I-V characteristic is given at biases exceeding μ_c by

$$\hbar I = g\Big(\mu - \frac{g}{g_{qp}+g}\sqrt{\mu^2 - \mu_c^2}\Big). \tag{11}$$

As discussed previously $\hbar\langle\dot{\phi}\rangle$ is the chemical potential difference between layers measured by four-terminal voltage probes. If the transport current flows at the outer edge, it can be directly measured in a Corbino geometry by placing voltage probes at the inner edge of the device. The resulting I-V characteristics, illustrated in Fig. 2, display cusp-like features near a critical bias as observed experimentally [47–49, 51] [61]. These cusp like features are absent [51] in the theory of Ref. 41. The values of Δ, g and g_{qp} appropriate to a particular sample can be extracted simply by measuring the critical current, the critical voltage, and the interlayer voltage in the dynamic regime. All experimental data of which we are aware can

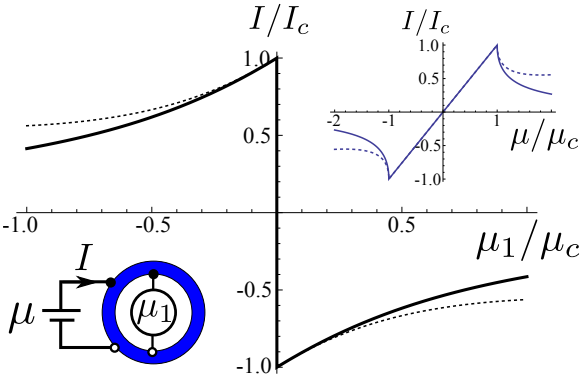


FIG. 2. (color online) Tunneling I-V characteristics in the macrospin limit. The lower inset provides a schematic illustration of the measurement geometry. The filled black and empty white dots represent top and bottom layer contacts respectively. μ/e (plotted in the inset) is the source to drain bias voltage, and $\mu_1/e = \hbar\langle\dot{\phi}\rangle/e$ is the interlayer voltage measured at the inner edge when the tunneling current flows at the outer edge. The solid lines are for the limit $g_{qp} \to 0$ and the dashed lines are for $g_{qp} = 0.2g$.

be accurately described in terms of these three parameters, although we expect small deviations in the dynamic regime because of the established non-ohmic character of incoherent interlayer tunneling in the quantum Hall regime.

Now we consider the experimental situation in which two sources inject independent tunneling currents I_i and I_o into the inner and outer edges of the Corbino device simultaneously [50, 51]. We count both currents as positive when electrons are injected into the top layer and collected from the bottom layer. The rates of pseudospin transfer in Eq. (8) add up: $\sum_k l_k I_k/2 = I_i + I_o$. Therefore, the criterion for the existence of a time independent condensate phase is simply: $|I_i + I_o| < I_c$. Quasiparticle transport at inner and outer edges is characterized by $\hbar I_{i,o} = g_{i,o}(\mu_{i,o} - \hbar\dot{\phi})$, with $g_{i,o}$ and $\mu_{i,o}$ the conductances (in $e^2/\hbar$ units) and the chemical potential biases driving the currents at each edge. Note that the effective bias reduction, $-\hbar\dot{\phi}$, is identical at inner and outer edges because condensate phase precession is spatially uniform in the macrospin limit. Figure 3 illustrates predictions of the macrospin theory for this experimental geometry. These curves are in good agreement with experiment [50, 51] and in particular capture two essential properties of the I-V characteristics measured in this situation: i) cusps in the I-V curves occur at a fixed value of $I_i + I_o = \mu_i/g_i + \mu_o/g_i$ and ii) conductance measured at the outer edge is larger in the dynamic regime in the present geometry than in the tunneling ($g_i \to 0$) limit. The latter property can be understood by viewing the conducting link between the upper and lower layers at the inner edge as a contribution to incoherent tunneling. The former property directly establishes the applicability of the macrospin limit. This connection will be made more explicit in Section IV where we calculate critical

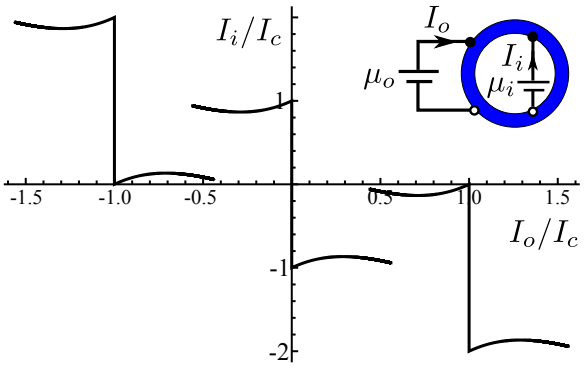


FIG. 3. Non-local coupling between tunneling at the inner and outer edges of a Corbino geometry sample in the macrospin limit. The three curves correspond are for bias sweeps at the outer edge μ_o at three different fixed biases in the inner edge: $\mu_i = \{-\mu_c, 0, \mu_c\}$. In the static regime $I_i = g\mu_i$ is independent of μ_o and $I_o = g\mu_o$. In the dynamic regime I_i decreases with increases in μ_o because $\langle\dot{\phi}\rangle$ increases. For this illustration we have taken $g_{qp} \to 0$, and $g_i = g_o = g$. The inset schematically illustrates the measurement geometry. The filled black and empty white dots represent top and bottom layer contacts respectively.

lines in the $I_i - I_o$ plane for λ smaller than sample sizes. Although surprising for reasons explained below, the conclusion that current samples are in the macrospin limit is inescapable.

The drag and series counterflow geometries identified in Ref. [35] are special cases of the two bias configurations described above, and are also successfully described by our theory. Consider first the nearly perfect counterflow Coulomb drag observed in the experiments of Ref. [9]. In these experiments a current I_1 is driven through the top layer between the inner and outer edges of a corbino annulus (drive current), while a current I_2 is measured between the inner and outer edges of the bottom layer (drag current). The experiment found that I_1 and I_2 are nearly equal in magnitude and oppositely directed. When the conductivity σ_{xx} of the quantum Hall bulk is zero, the only quasiparticle transport path consists of tunneling from top to bottom at the outer edge by interacting with the condensate, followed by current flow through the conducting link between the inner and outer edges of the bottom layer, followed by tunneling from bottom layer to top layer by interacting once again with the condensate. It follows that $I_1 = I_2$; the small difference observed experimentally is easily accounted for by imperfect insulating behavior of the quantum Hall bulk (i.e. by σ_{xx} having a small non-zero value). In this configuration the total rate of layer-pseudospin injected into the bilayer vanishes, i.e. $\sum_k l_k I_k/2 = 0$. Therefore the condensate phase remains static and close to its equilibrium value: $\phi = 0$ up to large currents. The equality of the drive and drag currents follows from the layer delocalized character of edge states in the presence of the condensate which produces an effective short-circuit between the drive and drag loops at the edges.

In the series counterflow configuration investigated in Ref. [49], the sample was a Hall bar. A current I is driven by a bias voltage μ/e between source and drain contacts to top and bottom layers at one end of the Hall bar and a conducting link between top and bottom layers is provided at the other end of the Hall bar. (See inset in Fig. 4). The source current and bias are related by $\hbar I = g(\mu - \hbar\dot{\phi})$, with g_L the two-terminal conductance measured between source and drain contacts in the absence of the loop resistor. The chemical potential drop across the loop resistor, μ_l is related to the loop current, I_l, by Ohm's law: $\hbar I_l = R\mu_l$, with R the loop resistance in units of $\hbar/e^2$. This chemical potential difference determines the tunneling current driven into the bilayer by the loop via: $\hbar I_l = -g_l(\mu_l - \hbar\dot{\phi})$ [62], with g_l the two-terminal conductance of the bilayer measured at the loop contacts (ideally e^2/h). This implies that the loop current directly probes of the condensate precession rate:

$$\dot{\phi} = (R + g_l^{-1})I_l. \tag{12}$$

Combining these equations with the property that net layer pseudospin transfer is $\sum_k l_k I_k/2 = I - I_l$, one obtains the behavior illustrated in Fig. 4, in agreement with experiment. For currents below the critical current, the finite loop resistor plays no role and the I-V characteristic is identical to that of a two-contact tunneling geometry. When the critical current is exceeded, a steady state is established in which $\hbar\dot{\phi}$ drives a quasiparticle current from bottom to top at the right end of the Hall bar which is completed by current flowing through the external loop.

Our theory also explains all other transport anomalies in a very simple manner. In the Hall drag measurement [4] current flows between source and drain contacts connected along the same edge and to the same layer, the drive layer. Because both contacts are made to the same layer, there is no net pseudsopin transfer torque and the order is always static. All voltage measurements, including in particular Hall voltage measurements, would measure a value that is independent of the contacting layer. The Hall voltage in particular has the same value in the drag layer and the drive layer, in agreement with experiment. The Hall voltages measured in series counterflow experiments [6, 7] vanish because the net current carried along the Hall bar is zero. In these experiments, voltage probes obtain non-zero values equal to $\hbar\langle\dot{\phi}\rangle/e$ in magnitude only when attached to opposite layers.

IV. CRITICAL CURRENTS FOR FINITE CONDENSATE STIFFNESS

For systems with larger values of Δ or smaller values of ρ the length scale λ which determines the typical distance over which the condensate phase changes can become smaller than the system size and the macrospin picture will no longer be appropriate. In this section

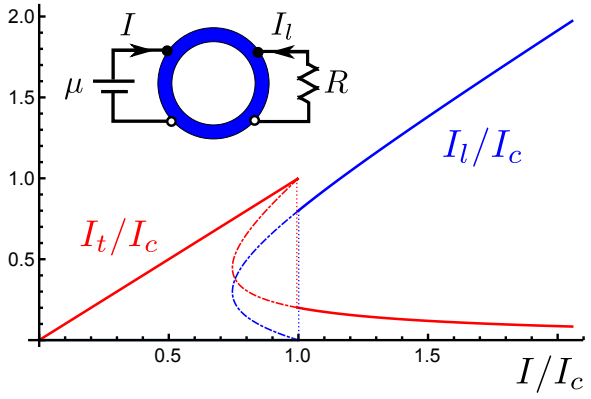


FIG. 4. (color online) Series counterflow measurement. The inset depicts the measurement configuration. The filled black dots and the empty white dots represent top and bottom layer contacts respectively. The tunneling current, defined as $I_t \equiv I - I_l$, is shown in red and the loop current, I_l, in blue. The dashed dotted lines indicate ranges over which the curves are multivalued. We have taken $g_{qp} \to 0$, and $g = g_l = 1/R$ for this illustration. In the low bias voltage regime $I_l = 0$ whereas in the high bias voltage regime $I_l \approx I$. The steady state established at high bias voltages is one in which $\hbar\dot{\phi}$ drives almost all the current through the loop resistor.

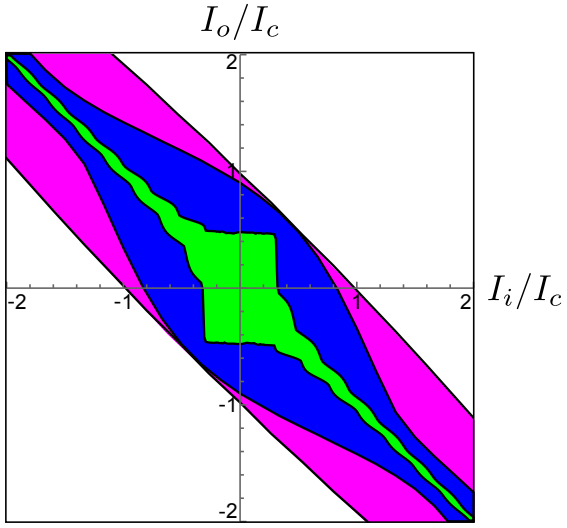


FIG. 5. (color online). Area in the $I_i - I_o$ parameter space for which a static condensate steady state exists. The three different regions correspond to $\lambda = R_i$ (purple), $R_i/2$ (blue), $R_i/5$ (green), and the Corbino ring was chosen to have $R_o = 2R_i$. For $\lambda = R_i$ the macrospin description is already accurate.

we explore the regime in which the phase changes substantially across the sample. One immediate conclusion from this study is that results for this limit are inconsistent with the measurements of Refs. [50, 51]. Specifically, we find that the boundary of the stability region for solutions with time independent condensate phase differs dramatically from the region $|I_i + I_o| = I_c$, predicted in the macrospin limit and found experimentally in Corbino device [50, 51] measurements.

When the length scale λ is smaller than the system size, determining the critical currents requires detailed modeling of the sample geometry and in particular of the spatial arrangement of the contacts [63]. For simplicity we employ a toy model of current injection by assuming that the tunneling current injection and exciton creation and annihilation occur uniformly along inner and outer Corbino edges with radii R_i and R_o. This geometry is easier to analyze because any dependence on azimuthal angle is ruled out by symmetry. In this case Eq. 6 reduces to:

$$\frac{\lambda^2}{r}\frac{d}{dr}\left(r\frac{d\phi}{dr}\right) = \sin\phi, \tag{13}$$

and the boundary conditions from Eq. 5 reduce to:

$$\left.\frac{d\phi}{dr}\right|_{R_o} = \frac{\hbar I_o}{4\pi\rho R_o}, \quad \left.\frac{d\phi}{dr}\right|_{R_i} = -\frac{\hbar I_i}{4\pi\rho R_i}. \tag{14}$$

The Neumann boundary conditions at inner and outer edges are sufficient to select a unique solution to the second order differential equation for $\phi(r)$. For some values of the currents at the inner and outer edges, I_i, I_o, there are no solutions to Eq. (13). Whenever this is true, the condensate must be time-dependent. Figure 5 plots, for several value of λ, the boundary of the region in the $I_o - I_i$ plane over which the condensate is able to reach a time independent steady state for several different values of λ. When currents are expressed in units of the macrospin critical current I_c, the stability region is largest for the largest values of λ. We see from Figure 5 that the macrospin limit is accurately approached already at $\lambda \sim R$. Since λ is reduced by increasing the strength of interlayer tunneling Δ_{SAS}, a change that can be experimentally implemented by slightly reducing the interlayer barrier thickness, it should be possible to test the deviations from the criterion $|I_o + I_i| < I_c$ experimentally. Deviations from the simple macrospin stability criterion, $|I_o + I_i| < I_c$, will signal the departure from the macrospin limit as illustrated in Fig. 5. Measurements of this type combined with detailed modeling of the sample geometry can be used to experimentally estimate the condensate stiffness ρ.

V. TIME-DEPENDENT TRANSPORT CHARACTERISTICS

The tunneling I-V characteristics described so far were obtained by averaging the precession rate of the condensate phase and the transport currents over time. They therefore correspond to *d.c.* measurements. However, above the critical bias where the condensate phase starts to precess the current can have an a.c. component in response to a d.c. bias. Therefore a.c. current measurements can provide additional information on the condensate dynamics.

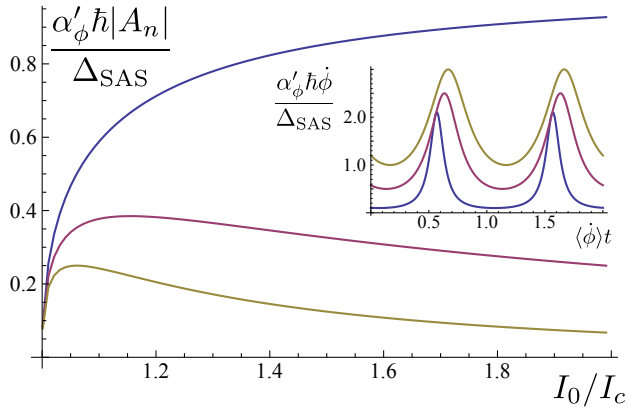


FIG. 6. In the time-dependent regime of a tunneling experiment the periodic precession rate of the condensate phase leads to a periodic contribution to the interlayer current. This figure plots harmonics of the precession rate of the condensate as a function μ/μ_c, which can be measured as an a.c. voltage in the inner rim of the Corbino annulus. Here $A_1^0 \equiv g\mu_c/(g_{qp}+g)$.

Equation (8) can be analytically solved for the instantaneous condensate precession rate. When the bias exceeds the critical value, $\mu > \mu_c \equiv \hbar I_c/g$:

$$\hbar\dot\phi = \left(\frac{g\mu}{g_{qp}+g}\right)\frac{(\mu^2-\mu_c^2)\sec^2(\langle\dot\phi\rangle t/2)}{\mu^2+[\mu_c+\sqrt{\mu^2-\mu_c^2}\tan(\langle\dot\phi\rangle t/2)]^2} \tag{15}$$

where $\langle\dot\phi\rangle$ is given by Eq. (10). For biases that barely exceed the critical value, $\mu \gtrsim \mu_c$, $\dot\phi$ oscillates in a very anharmonic fashion. Figure 6 illustrates the amplitudes, $|A_n|$, of the leading harmonics of the condensate precession rate, *i.e.* $\hbar\dot\phi = A_n e^{in\langle\dot\phi\rangle t}$, with the fundamental frequency given by the average precession rate $\langle\dot\phi\rangle$ from Eq. (10). Interestingly, in the limit $\mu \gg \mu_c$ all higher harmonics die out, $A_n \to 0$ for $n \geq 2$, but the fundamental harmonic remains finite with an amplitude given by: $A_1 \to A_1^0 \equiv g\mu_c/(g_{qp}+g)$. Thus the rate of precession becomes sinusoidal:

$$\hbar\dot\phi \approx \frac{g}{g+g_{qp}}\left[\mu - \mu_c\cos(\langle\dot\phi\rangle t)\right], \quad \mu \gg \mu_c. \tag{16}$$

Another interesting case is that of driving voltages with a finite a.c. component: $\mu + \delta\mu\sin(\omega t)$. With an applied bias of this form the I-V characteristics display the analog of the Shapiro steps [43] that are observed in Josephson junctions [64]. In this regime, the average precession rate will lock at discrete values which are integer multiples of the driving frequency, *i.e.* $\langle\dot\phi\rangle = k\omega$ with $k \in \mathbb{Z}$ over finite intervals of the average driving voltage μ as illustrated in the insets of Figs. 7(a)-(b). Consequently the average d.c. voltage measured at the inner rim of the Corbino annulus will remain fixed at discrete values $-k\hbar\omega$, over finite ranges of the average driving voltage μ. The width

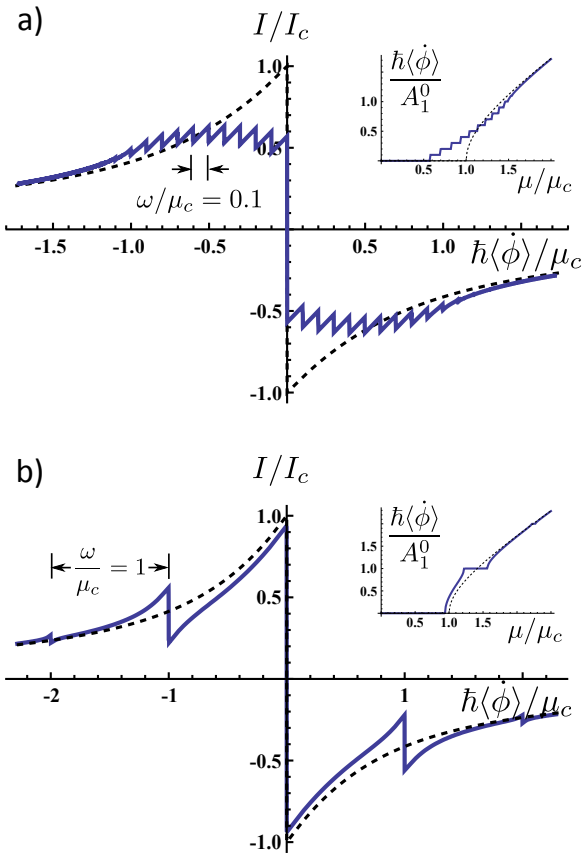


FIG. 7. (color online) Illustration of the Shapiro steps that arise when an a.c. signal is added to the d.c. bias. Panel a) corresponds to a driving frequency $\hbar\omega = 0.1\mu_c$, and panel b) to $\hbar\omega = \mu_c$. In both cases the amplitude of the oscillating bias was taken to be $\delta\mu = \mu_c/2$. The insets illustrate the behavior of the averaged precession rate of the condensate, which is proportial to the tunneling voltage measured in the inner edge of the Corbino ring. The dashed black lines correspond to the behavior for pure d.c. bias illustrated in Fig. 2. We chose $g_{qp} \to 0$.

TABLE I. Widths of the Shapiro steps in the limit of slow driving frequencies and small driving amplitudes.

$k \in \mathbb{Z}$	$\Delta\mu_k/\mu_c$
0	$2 - 2\frac{\delta\mu}{\mu_c} + 2\left(1+\frac{g_{qp}}{g}\right)\frac{\hbar\omega}{\mu_c}\sqrt{\frac{\delta\mu}{\mu_c}}$
1	$2\left(1+\frac{g_{qp}}{g}\right)\frac{\hbar\omega}{\mu_c}\sqrt{\frac{\delta\mu}{\mu_c}}$
2	$2\left(1+\frac{g_{qp}}{g}\right)\frac{\hbar\omega}{\mu_c}\sqrt{\frac{\delta\mu}{\mu_c}}$

of the k-th step, $\Delta\mu_k$, is controlled by the amplitude of a.c. component of the driving voltage $\delta\mu$. Approximate expressions for the values of the widths of the first steps in the limit of slow driving frequencies ($\hbar\omega \ll \mu_c$) and small driving amplitudes ($\delta\mu \ll \mu_c$), derived in Ref. 65, are listed in Table I.

The widths of the steps in the opposite limit of fast driving frequencies, $\hbar\omega \gg \mu_c, \delta\mu$, can be shown to be given by:

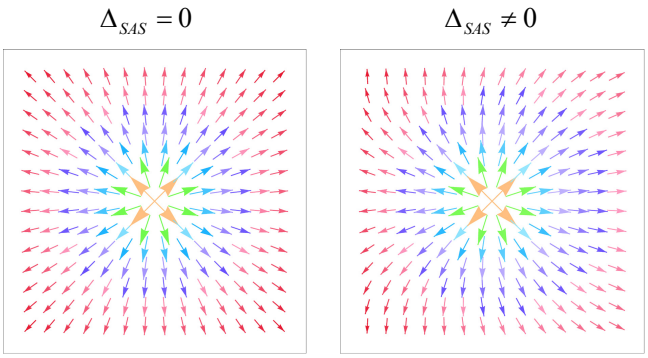


FIG. 8. (color online) Illustration of the impact of interlayer tunneling near a meron core. The right panel depicts how the presence of a weak tunneling term, which breaks the XY symmetry, produces a well defined spatially averaged phase.

$$\Delta\mu_k = 2\ \mu_c\ J_k \left[\frac{\delta\mu}{\hbar\omega(1+g_{qp}/g)}\right], \tag{17}$$

with J_k the k-th Bessel function [64, 65].

The critical currents in recent samples are on the order of $eI_c \sim 1$nA [50, 51]. To realize discernible steps it is desirable that the applied bias frequency reaches values no more than an order of magnitude smaller than I_c. This means that the desired frequencies are $\omega \gtrsim 10$GHz should be attainable by pure electronic means. It might also be interesting to explore the coupling of the condensate to microwave radiation. Note that the predictions made here for Shapiro step widths differ qualitatively from those in Ref. 43, allowing future experiments to distinguish between the two different theoretical frameworks.

VI. IMPACT OF DISORDER

We have demonstrated that the assumption of a long-ranged nearly uniform order in coherent quantum Hall bilayers is able to explain all the surprising transport anomalies that this system displays. We have so far adopted a mainly phenomenological viewpoint and have not addressed in detail the microscopic physics which determines the values of the coupling constants in the order parameter energy functional. We now propose a physical interpretation of the phase variable in our theory which extends previous arguments [40, 42] that disorder drastically reduces the strength of the coupling of interlayer tunneling to the condensate.

Consider first the case of a bilayer with purely spontaneous interlayer phase coherence in the absence of interlayer tunneling. The strength of order in such a system is reduced by quantum and thermal fluctuations. These effects have been addressed by many researchers, but are ignored below because their impact is [40, 42] insufficient to explain the reduction in the strength of interlayer tunnel coupling to the condensate by four to five orders of magnitude found in experiments [3]. We concentrate instead on the influence of disorder, which couples to the interlayer phase because of the relationship [21, 66] in quantum Hall systems between pseudospin textures and charge density. Smooth local density variations $n(\vec{r})$ are generated in quantum Hall ferromagnets when the spatial gradients of both the interlayer phase (φ) and the layer polarization (M_z) are non-zero [21, 66]:

$$\delta n(\vec{r}) = -\frac{1}{4\pi}\hat{M}(\vec{r})\cdot[\partial_x\hat{M}(\vec{r})\times\partial_y\hat{M}(\vec{r})]. \tag{18}$$

Smooth random potential variation, which is always present in high-mobility two-dimensional electron systems, therefore favors pseudospin textures and can [21] drive the formation of vortices and anti-vortices (merons) in the pseudospin order parameter. Current experiments can be understood under the assumption that disorder in the absence of interlayer tunneling is sufficient to completely destroy long range order in the interlayer phase. This is a natural assumption because of the relationship between disorder potentials and pseudospin textures.

We refer to the interlayer phase configuration which minimizes the sum of the disorder energy,

$$E_{dis} = \int d^2\vec{r}\, n(\vec{r})\, V_{dis}(\vec{r}), \tag{19}$$

and the pseudospin stiffness energy,

$$E_{rho} = \rho \int d^2\vec{r}\ |\nabla\varphi(\vec{r})|^2, \tag{20}$$

as $\varphi_0(\vec{r})$. In writing the gradient energy in this form we are assuming that the pseudospin lies in its $\hat{x}-\hat{y}$ plane with local azimuthal orientation $\varphi(\vec{r})$ except near small meron (vortex) cores. Because long-range phase order is absent in the absence of inter-layer tunneling we have:

$$\begin{aligned}
\langle\cos(\varphi_0(\vec{r}))\rangle_{\vec{r}} &= 0,\\
\langle\sin(\varphi_0(\vec{r}))\rangle_{\vec{r}} &= 0,\\
\langle\cos^2(\varphi_0(\vec{r}))\rangle_{\vec{r}} &= 1/2,\\
\langle\sin^2(\varphi_0(\vec{r}))\rangle_{\vec{r}} &= 1/2.
\end{aligned} \tag{21}$$

where the angle brackets denote spatial averages. Because only phase gradients yield charge densities, disorder determines the interlayer phase only up to a global constant. The characteristic length scale for variations in $\varphi_0(\vec{r})$ is the disorder correlation length ξ.

Now consider how the ground state phase configuration is altered when interlayer tunneling is present. Because the interlayer tunneling explcitly breaks the global XY symmetry, the system can develop a global phase even after spatially averaging, as illustrated in Fig. 8. The interlayer tunneling energy is:

$$E_{tun} = -n\Delta_{SAS}\int d^2\vec{r}\cos(\varphi(\vec{r})). \tag{22}$$

In the pseudospin language, the interlayer tunneling produces a spatially constant effective magnetic field which acts in the $\hat{x}$ direction and has magnitude Δ_{SAS}. In the same language $\varphi_0(\vec{r})$ describes the orientation of a pseudospin that is aligned with a spatially varying pseudospin effective magnetic field with a typical magnitude $\sim \rho/n\xi^2$, which is much larger than Δ_{SAS}. Here $n = (2\pi\ell^2)^{-1}$ is the full Landau level density and the factor of n in the denominator renormalizes energy per area to energy per electron. The additional weak field will result in a shifted ground state interlayer phase,

$$\varphi_{GS}(\vec{r}) = \varphi_0(\vec{r}) + \delta\varphi(\vec{r}), \tag{23}$$

where $\delta\varphi(\vec{r})$ is describes the reorientation of pseudo-spins towards the $\hat{x}$ direction. The phase shift is largest in magnitude when the unperturbed pseudospin is perpendicular to the $\hat{x}$ direction, and has a typical magnitude proportional to the ratio of the two fields. It follows that $\delta\varphi \ll 1$, and that:

$$\delta\varphi(\vec{r}) \sim -\frac{\Delta_{SAS} n\xi^2 \, \sin(\varphi_0(\vec{r}))}{\rho}, \tag{24}$$

and hence that:

$$\begin{aligned} \langle \cos(\varphi_{GS}(\vec{r}))\rangle_{\vec{r}} &\sim \frac{\Delta_{SAS} n\xi^2}{2\rho}, \\ \langle \sin(\varphi_{GS}(\vec{r}))\rangle_{\vec{r}} &= 0. \end{aligned} \tag{25}$$

Let us now consider the influence of the transport bias voltages and the pseudospin transport torques. In the presence of transport currents the condensate phase is given by:

$$\varphi(\vec{r}) \to \varphi_{GS}(\vec{r}) + \phi(\vec{r}), \tag{26}$$

where $\phi(\vec{r})$ describes the local deviation from the equilibrium orientation in the presence of the tunneling term. We will argue that $\phi(\vec{r})$ should be identified with the phase variable employed in the main body of this paper and that it is very slowly varying so that it does not contribute significantly to the pseudospin-texture related charge density. In particular, the dependence of total energy on $\phi(\vec{r})$ can be found to be given:

$$E[\phi] \approx E_{GS} - \int d^2\vec{r} \, [\Delta \cos(\phi(\vec{r})) + \rho |\nabla\phi(\vec{r})|^2], \tag{27}$$

with:

$$\Delta = \Delta_{SAS} n \langle \cos(\varphi_{GS}(\vec{r}))\rangle_{\vec{r}} \sim \frac{(n\xi\Delta_{SAS})^2}{2\rho}. \tag{28}$$

Equation (27) applies provided that ϕ varies slowly on the disorder length scale ξ and is based on the observation that $\langle \nabla\varphi_{GS}(\vec{r})\rangle_{\vec{r}} = 0$ because there is no macroscopic exciton flow in the absence of electrical bias voltages. The final conclusion is that in Eq. (3) the effective stiffness parameter ρ is not strongly influenced by disorder, but the the effective interlayer tunneling parameter is strongly suppressed from $n\Delta_{SAS}$ to $\Delta \sim (n\xi\Delta_{SAS})^2/(2\rho)$.

Let us now illustrate how this picture is in quantitative agreement with experiments. In the early experiments of Spielman *et al.*, the typical value of the tunneling amplitude was estimated to be $\Delta_{SAS} \sim 10^{-9}$eV [46]. The stiffness energy scale at $d = 0$ is $\rho = (e^2/\epsilon l)/(32\sqrt{2\pi}) \sim 10^{-4}$eV [21, 66]. In mean-field theory, the stiffness is reduced by a further factor of ~ 3 at the values of d/ℓ studied experimentally and quantum fluctuations [26] can reduce the stiffness further. The macrospin critical current one would naively expect in the absence of disorder for these samples, which have an area $A \sim 250 \times 250\mu\text{m}^2$, is about $eI_c \sim 10^{-7}A$. However, these experiments found a critical current about four orders of magnitude smaller: $eI_c \sim 10^{-11}$A [46]. The relative smallness of this critical current is a signature of the strongly reduced effective tunneling amplitude. Estimating the impact of disorder requires knowledge of the typical values for the disorder correlation length. As we argue below, in-plane field measurements of the critical current are consistent with a value of the disorder correlation length of about $n\xi^2 \sim 10$. With this estimate one obtains that the critical current is expected to be reduced to about $eI_c \sim 10^{-11}$A, in agreement with experiment. Furthermore, using paramters from more recent experiments with larger tunneling amplitudes of about $\Delta_{SAS} \sim 10^{-8}$eV [48], the mechanism described in this section predicts an enhanced critical current of about $eI_c \sim 10^{-9}$A, which is again in agreement with their findings. We therefore conclude that this mechanism is the main factor behind the dramatic reduction of the critical current.

The property that the critical current is proportional to the square of the microscopic interlayer tunneling amplitude Δ_{SAS} is consistent with experiment, including very recent measurements [52] which compared similar samples with different tunnel-barrier thicknesses, although very precise comparisons require measurements at current values close to the critical value and are therefore challenged by circuit instabilities. Uncontrolled wafer-scale spatial variation in the tunnel barrier thickness can [3] also complicate comparison between theory and experiment.

We would like now to discuss the implications of this picture for in-plane field measurements. In pseudospin language, an in-plane magnetic field causes the effective magnetic field due to tunneling to precess around the $\hat{z}$ axis, instead of being fixed in the $\hat{x}$ direction. The azimuthal orientation of the pseudo spin field is [21] $\phi_B = Qx$ where $Q = 2\pi B_\parallel d/\Phi_0$, d is the layer separation, Φ_0 is the magnetic flux quantum, and x is the planar coordinate perpendicular to the in-plane magnetic field direction. If the macrospin limit were achieved in the absence of disorder, the condensate stiffness would suppress its phase response to the precessing in-plane field. The condensate would then couple only to the spatial average average of the in-plane field, yielding a

Fraunhofer pattern analogous to that found in Josephson junctions. For QL large compared to system-size, the critical current should be strongly reduced. In contrast the experimental finding is that the critical current is reduced only gradually and at a field scale corresponding to $Q^{-1} \sim 0.1\mu$m [45, 46, 52], which is smaller than the sample sizes typically used in bilayer exciton condensate studies. The picture outlined above also provides a simple explanation for the unexpectedly weak dependence of tunneling transport anomalies on in-plane magnetic fields. Instead of being reoriented toward the $\hat{x}$ direction by tunneling, the pseudospin will be reoriented toward the local effective field direction. Eq. (22) is therefore modified to:

$$E_{tun} = -\frac{\Delta_{SAS}}{2\pi\ell^2}\int d^2\vec{r}\cos(\varphi(\vec{r}) - Qx), \qquad (29)$$

and Eq. (24) to:

$$\delta\varphi(\vec{r}) \sim -\frac{\Delta_{SAS} n\xi^2 \sin(\varphi_0(\vec{r}) - Qx)}{\rho}, \qquad (30)$$

but Eq. (27) is unaltered. Changes are expected in an in-plane magnetic field only when $Q\xi \gtrsim 1$. In-plane field dependent measurements therefore allow one to extract a value for the disorder correlation length of about $\xi \sim 0.1\mu$m.

The ideas discussed in this paper can be tested experimentally by increasing the bare microscopic interlayer tunneling amplitude sufficiently to escape from the macrospin limit. The length-scale $\lambda = \sqrt{2\rho/\Delta}$ over which variations of the coarse grained phase ϕ occur, can be estimated by using the experimentally measured critical currents to be about $\sim 1mm$ for the samples described in Ref. [46], and about $\sim 0.1mm$ in the samples of Ref. [48]. In the presence of disorder one expects λ to be inversely proportional to the bare tunneling amplitude, $\lambda \sim 2\rho/(n\xi\Delta_{SAS})$. Because Δ_{SAS} is exponentially sensitive to both the height (*i.e.* to the Al fraction) and the width of the tunnel barrier between quantum wells, there does not seem to be a serious obstacle to increasing the critical current by increasing Δ_{SAS}, while reducing λ. By increasing Δ_{SAS} by about an order of magnitude with respect to current values reported in Refs. [48, 51] one should be able to attain the conditions in which the deviations from the macrospin limit illustrated in Fig. 5. are observable.

VII. SUMMARY AND DISCUSSION

We have demonstrated that a satisfactory understanding of all transport anomalies associated with the exciton condensate state of quantum Hall bilayers [3] can be achieved by combining a fermion mean-field quasiparticle theory of transport with a theory of the condensate which accounts for its response [35] to quasiparticle excitonic Andreev scattering. This theory is closely related to the picture successfully used to describe magneto-electronic effects in circuits containing magnetic metals. It uses the same framework to explain anomalous interlayer tunneling, quantized Hall drag, the absence of a Hall voltage in Hall bar counterflow measurements, and perfect Coulomb drag and non-local coupling between tunneling at inner and outer edges in Corbino geometry bilayers. Using this theory we have shown that recent measurements in Corbino devices [50, 51] directly demonstrate that samples studied to date are in a macrospin limit in which the condensate stiffness is sufficient to maintain a spatially constant value of the coarse grained condensate phase. The constant phase is unexpected because interlayer tunneling strongly favors interlayer phases which return to zero away from current source and drain contacts over a length scale that is naively expected to be much smaller than the system size. We have argued, however, that the phase that enters in the macrospin model must be interpreted as a coarse grained average of a local interlayer phase that is strongly scrambled by disorder because of the relationship [21, 66] between charge densities and pseudospin textures in the quantum Hall regime. Using this idea we can explain a strong reduction of the effective interlayer tunneling strength by about four orders of magnitude from the naive value extracted from the bare tunneling amplitude: the reduction explains the applicability of the macrospin limit, the small experimental values of the tunneling anomaly critical currents, and the surprising weak dependence of tunneling on in-plane magnetic field. We have applied the theory to predict anomalies in *ac* transport measurements, and to predict changes in the non-local relationship between tunneling characteristics at inner and outer Corbino sample edges in devices with stronger interlayer tunneling than has been studied to date. Specifically we predict that the experimental finding that the critical current for the tunneling anomaly is the sum of the currents at the two Corbino edges will break down in samples with stronger interlayer tunneling [3].

Our main goal in this paper is to lay out a theoretical framework for treating the transport properties of bilayer exciton condensate. In order to focus on this goal we have neglected some details which do play an experimental role. In particular we have concentrated on the zero-temperature limit by assuming a perfect quantum Hall effect and by neglecting thermal fluctuations of the condensate. Only when the quantum Hall effect is perfect is our assumption that quasiparticles travel ballistically between source, drain, and voltage contacts on the same sample edge - and never between contacts on opposite edges - exactly valid. The property that a perfect quantum Hall effect is approached as $T \to 0$ makes quasiparticle transport in this limit very simple and allows our theoretical framework to be directly tested. However, the theory is very readily generalized to account for an imperfect quantum Hall effect. Similarly thermal condensate fluctuations can readily be accounted for our theory by adding a stochastic contribution to the

condensate equation of motion that is consistent with the fluctuation-dissipation theorem and with the model used for dissipative incoherent quasiparticle tunneling between layers. Finally, there is good reason to expect quasiparticle-tunneling to be both non-Ohmic and temperature-dependent. The Ohmic tunneling assumption is adopted here for illustrative purposes only.

Achieving a complete understanding of transport in quantum Hall bilayers is not only of fundamental interest, but also useful for gaining insight into transport in systems that at first glance appear to be quite different but which share crucial similarities. Indeed, we have recently exploited the similarity between coherent bilayers and easy-plane ferromagnets to propose a new kind of spintronic device that displays non-local coupling between spatially separated transport channels [57] that is analogous to that displayed by the Corbino geometry samples explored in this paper. Understanding similarities and differences between these kind of systems might prove useful in advancing both fundamental and applied condensed matter physics research.

ACKNOWLEDGMENTS

We are grateful to W. Dietsche, J.P. Eisenstein, B.I. Halperin, K. von Klitzing, and D. Zhang for valuable interactions. This work was supported by DOE Division of Materials Sciences and Engineering grant DE-FG03-02ER45958 and Welch Foundation grant TBF1473. I.S. acknowledges the support of the Pappalardo Fellowship in Physics.

[1] I. B. Spielman, J. P. Eisenstein, L. N. Pfeiffer, and K. W. West, Phys. Rev. Lett. **84**, 5808 (2000).
[2] J. Eisenstein and A. MacDonald, Nature **432**, 691 (2004).
[3] J. Eisenstein, Annual Review of Condensed Matter Physics **5**, 159 (2014).
[4] M. Kellogg, I. B. Spielman, J. P. Eisenstein, L. N. Pfeiffer, and K. W. West, Phys. Rev. Lett. **88**, 126804 (2002).
[5] M. Kellogg, J. P. Eisenstein, L. N. Pfeiffer, and K. W. West, Phys. Rev. Lett. **93**, 036801 (2004).
[6] E. Tutuc, M. Shayegan, and D. A. Huse, Phys. Rev. Lett. **93**, 036802 (2004).
[7] R. D. Wiersma, J. G. S. Lok, S. Kraus, W. Dietsche, K. von Klitzing, D. Schuh, M. Bichler, H.-P. Tranitz, and W. Wegscheider, Phys. Rev. Lett. **93**, 266805 (2004).
[8] A. D. K. Finck, J. P. Eisenstein, L. N. Pfeiffer, and K. W. West, Phys. Rev. Lett. **106**, 236807 (2011).
[9] D. Nandi, A. Finck, J. Eisenstein, L. Pfeiffer, and K. West, Nature **488**, 481 (2012).
[10] H. A. Fertig, Phys. Rev. B **40**, 1087 (1989).
[11] J. P. Eisenstein, G. S. Boebinger, L. N. Pfeiffer, K. W. West, and S. He, Phys. Rev. Lett. **68**, 1383 (1992).
[12] S. Q. Murphy, J. P. Eisenstein, G. S. Boebinger, L. N. Pfeiffer, and K. W. West, Phys. Rev. Lett. **72**, 728 (1994).
[13] A. H. MacDonald, P. M. Platzman, and G. S. Boebinger, Phys. Rev. Lett. **65**, 775 (1990).
[14] L. Brey, Phys. Rev. Lett. **65**, 903 (1990).
[15] X.-G. Wen and A. Zee, Phys. Rev. Lett. **69**, 1811 (1992).
[16] X. G. Wen and A. Zee, Phys. Rev. B **47**, 2265 (1993).
[17] O. Narikiyo and D. Yoshioka, Journal of the Physical Society of Japan **62**, 1612 (1993).
[18] Z. F. Ezawa and A. Iwazaki, Phys. Rev. B **47**, 7295 (1993).
[19] K. Yang, K. Moon, L. Zheng, A. H. MacDonald, S. M. Girvin, D. Yoshioka, and S.-C. Zhang, Phys. Rev. Lett. **72**, 732 (1994).
[20] Z. Ezawa and A. Iwazaki, International Journal of Modern Physics B **08**, 2111 (1994).
[21] K. Moon, H. Mori, K. Yang, S. M. Girvin, A. H. MacDonald, L. Zheng, D. Yoshioka, and S.-C. Zhang, Phys. Rev. B **51**, 5138 (1995).
[22] K. Yang, K. Moon, L. Belkhir, H. Mori, S. M. Girvin, A. H. MacDonald, L. Zheng, and D. Yoshioka, Phys. Rev. B **54**, 11644 (1996).
[23] A. Stern, S. M. Girvin, A. H. MacDonald, and N. Ma, Phys. Rev. Lett. **86**, 1829 (2001).
[24] L. Balents and L. Radzihovsky, Phys. Rev. Lett. **86**, 1825 (2001).
[25] M. M. Fogler and F. Wilczek, Phys. Rev. Lett. **86**, 1833 (2001).
[26] Y. N. Joglekar and A. H. MacDonald, Phys. Rev. Lett. **87**, 196802 (2001).
[27] K. Yang, Phys. Rev. Lett. **87**, 056802 (2001).
[28] E. Demler, C. Nayak, and S. Das Sarma, Phys. Rev. Lett. **86**, 1853 (2001).
[29] A. Stern and B. I. Halperin, Phys. Rev. Lett. **88**, 106801 (2002).
[30] H. A. Fertig and J. P. Straley, Phys. Rev. Lett. **91**, 046806 (2003).
[31] D. N. Sheng, L. Balents, and Z. Wang, Phys. Rev. Lett. **91**, 116802 (2003).
[32] H. A. Fertig and G. Murthy, Phys. Rev. Lett. **95**, 156802 (2005).
[33] E. Rossi, A. S. Núñez, and A. H. MacDonald, Phys. Rev. Lett. **95**, 266804 (2005).
[34] K. Park and S. Das Sarma, Phys. Rev. B **74**, 035338 (2006).
[35] J.-J. Su and A. MacDonald, Nature Physics **4**, 799 (2008).
[36] P. R. Eastham, N. R. Cooper, and D. K. K. Lee, Phys. Rev. B **80**, 045302 (2009).
[37] D. V. Fil and S. I. Shevchenko, Journal of Physics: Condensed Matter **21**, 215701 (2009).
[38] F. Dolcini, D. Rainis, F. Taddei, M. Polini, R. Fazio, and A. H. MacDonald, Phys. Rev. Lett. **104**, 027004 (2010).
[39] P. R. Eastham, N. R. Cooper, and D. K. K. Lee, Phys. Rev. Lett. **105**, 236805 (2010).
[40] J.-J. Su and A. H. MacDonald, Phys. Rev. B **81**, 184523 (2010).
[41] T. Hyart and B. Rosenow, Phys. Rev. B **83**, 155315 (2011).
[42] D. A. Pesin and A. H. MacDonald, Phys. Rev. B **84**, 075308 (2011).
[43] T. Hyart and B. Rosenow, Phys. Rev. Lett. **110**, 076806

(2013).
[44] Y. Hama, G. Tsitsishvili, and Z. F. Ezawa, Progress of Theoretical and Experimental Physics **2013** (2013), 10.1093/ptep/ptt025.
[45] I. B. Spielman, J. P. Eisenstein, L. N. Pfeiffer, and K. W. West, Phys. Rev. Lett. **87**, 036803 (2001).
[46] I. B. Spielman, *Evidence for the Josephson Effect in Quantum Hall Bilayers*, Ph.D. thesis, Caltech (2004).
[47] L. Tiemann, W. Dietsche, M. Hauser, and K. von Klitzing, New Journal of Physics **10**, 045018 (2008).
[48] L. Tiemann, Y. Yoon, W. Dietsche, K. von Klitzing, and W. Wegscheider, Phys. Rev. B **80**, 165120 (2009).
[49] Y. Yoon, L. Tiemann, S. Schmult, W. Dietsche, K. von Klitzing, and W. Wegscheider, Phys. Rev. Lett. **104**, 116802 (2010).
[50] X. Huang, W. Dietsche, M. Hauser, and K. von Klitzing, Phys. Rev. Lett. **109**, 156802 (2012).
[51] D. Nandi, T. Khaire, A. D. K. Finck, J. P. Eisenstein, L. N. Pfeiffer, and K. W. West, Phys. Rev. B **88**, 165308 (2013).
[52] D. Zhang, X. Huang, W. Dietsche, M. Hauser, and K. von Klitzing, Phys. Rev. B **90**, 085436 (2014).
[53] This is a direct consequence of the fact that ϕ and M_z are canonically conjugated variables [16]: the Euler-Lagrange equation for M_z implies $\hbar\dot{\phi} = \delta\mathcal{E}/\delta M_z$, and the chemical potential difference between the layers is the energy cost of moving one electron from the bottom to the top layer, for which $\int d^2r\ \delta M_z = 1$.
[54] T. L. Gilbert, Magnetics, IEEE Transactions on **40**, 3443 (2004).
[55] M. Tinkham, *Introduction to superconductivity* (Courier Dover Publications, 2012).
[56] R. Prange and S. Girvin, eds., *The quantum Hall effect*, Vol. 1 (Springer-Verlag New York, 1987) Chap. 8.
[57] H. Chen, A. D. Kent, A. H. MacDonald, and I. Sodemann, arXiv preprint arXiv:1408.1100 (2014).
[58] Y. Tserkovnyak, A. Brataas, and G. E. W. Bauer, Phys. Rev. Lett. **88**, 117601 (2002).
[59] Y. Tserkovnyak, A. Brataas, G. E. W. Bauer, and B. I. Halperin, Rev. Mod. Phys. **77**, 1375 (2005).
[60] A. D. K. Finck, A. R. Champagne, J. P. Eisenstein, L. N. Pfeiffer, and K. W. West, Phys. Rev. B **78**, 075302 (2008).
[61] The system I-V curve has a region of negative differential resistivity at voltages immediately above the cusp which leads to circuit instabilities that make measurements extremely close to the maximum in the I-V curve difficult. Ref. 51 addressed this experimental challenge and provided a thorough characterization of the behavior of the I-V curve immediately above the critical current.
[62] The minus sign arises because the positive loop resistance sign convention has been redefined to be be positive when the number current is injected into the bottom layer to match the convention of Ref. [49].
[63] In this sense the very observation of the independence of the critical current on the contact position along the rim of the Corbino annulus is already an indication that λ is longer than the system size [51].
[64] C. C. Grimes and S. Shapiro, Phys. Rev. **169**, 397 (1968).
[65] M. Renne and D. Polder, Revue de physique appliquée **9**, 25 (1974).
[66] S. L. Sondhi, A. Karlhede, S. A. Kivelson, and E. H. Rezayi, Phys. Rev. B **47**, 16419 (1993).